Journal of Organometallic Chemistry, 461 (1993) 127–139

JOM 23721

Syntheses, structures, and spectroscopic properties of novel sulfurdiimine complexes; spectroscopic properties of the di-t-butylsulfurdiimine (DBSD) complexes $M(CO)_3Br(DBSD\text{-}N,N')$ (M = Mn, Re) and X-ray structures of the metal–metal bonded compounds $(CO)_8Mn_2(DBSD\text{-}N,N')$ and $(CO)_6Mn_2(\mu\text{-}DBSD\text{-}N,N':N,S,N')$

C. Mahabiersing [a], W.G.J. de Lange [a], K. Goubitz [b] and D.J. Stufkens [a]

[a] *Anorganisch Chemisch Laboratorium,* [b] *Laboratorium voor Kristallografie, Universiteit van Amsterdam, J.H. van 't Hoff Instituut, Nieuwe Achtergracht 166, 1018 WV Amsterdam (Netherlands)*

(Received January 1, 1993)

Abstract

The complexes $M(CO)_3Br(DBSD\text{-}N,N')$ (M = Mn or Re; DBSD = di-t-butylsulfurdiimine = $^tBu\text{-}N{=}S{=}N\text{-}^tBu$) have been prepared by reaction of $M(CO)_5Br$ with DBSD. The complexes have been characterized spectroscopically (^1H-NMR, IR, UV/Vis and resonance Raman) and used as starting materials for the preparation of the metal–metal bonded complexes $(CO)_8MM'(DBSD\text{-}N,N')$ (M,M' = Mn, Re). The structure of $(CO)_8Mn_2(DBSD\text{-}N,N')$ has been determined by X-ray crystallography. Both Mn atoms have slightly distorted octahedral geometry, and the Mn–Mn distance (2.967 Å) is longer than that in $Mn_2(CO)_{10}$ (2.9038 Å). The DBSD is bonded to Mn as a chelate in its *trans, trans*-conformation, and the N–S bond lengths and NSN bond angle are nearly the same as in $W(CO)_4(DBSD\text{-}N,N')$. The complexes $(CO)_8MM'(DBSD\text{-}N,N')$ are transformed thermally and photochemically into $(CO)_6MM'(\mu\text{-}DBSD\text{-}N,N':N,S,N')$; during this reaction the coordination of the DBSD ligand changes from chelate to bridging. This has been established by an X-ray structural study of $(CO)_6Mn_2(\mu\text{-}DBSD\text{-}N,N':N,S,N')$. Both Mn atoms possess a distorted octahedral geometry and the Mn–Mn distance (2.638 Å) is very short. The N–S bond distances are increased from ~ 1.60 Å in the unbridged complex to ~ 1.70 Å in this bridged species, which contains the longest N–S bond observed so far for a sulfurdiimine ligand. The mechanism of the photochemical formation of this complex is discussed.

1. Introduction

Coordination and activation of olefins by transition metals have been very important topics in organometallic and catalytic research. Coordination activates the olefins and initiates their chemical reactions in *e.g.* hydrogenation, polymerization, metathesis, and hydroformylation reactions. Similar double bond activation has been observed for heteroolefins containing N=C or N=S bonds such as 1,4-diaza-1,3-butadienes (R-DAB; R–N=CH–CH=N–R) [1–6], *N,N'*-substituted sulfurdiimines (R–N=S=N–R) [1,7] and sulfinylanilines (R–N=S=O) [17]. The R-DAB ligands in particular, showed a great variety of bonding modes, ranging from two-electron coordination via one nitrogen lone pair in $PdCl_2(PPh_3)(^tBu\text{-}DAB\text{-}N)$ [8] to eight-electron coordination in metal clusters such as $Ru_3(CO)_8(^nPent\text{-}DAB\text{-}N,N':N,C,C',N')$ [9,10]. In the latter case the ligand binds to one Ru-metal atom as a chelate via the two N-atoms and to another Ru centre in a η^4-coordination via the two imine (CH=N) groups. Intermediate cases in which the R-DAB ligand acts as a four- or six-electron donor ligand, have also been reported [11–13]. In contrast, the coordination modes of the sulfurdiimines R–N=S=N–R seemed to be restricted to those depicted in Fig. 1.

Even for these bonding modes, coordination via the S atom (Fig. 1e) has been established only for an intermediate in the fluxional movement of $M(CO)_5(RNSNR\text{-}N)$ (M = Cr, W) [14,15], while η^2-bonding (Fig. 1f) has also not been found in a stable complex. Thus, the complex $Pt(PPh_3)_2(ArNSNAr\text{-}N,S)$ (Ar = $3,5\text{-}Me_2C_6H_3$), in which the sulfurdiimine is η^2-bonded

Correspondence to: Dr. D.J. Stufkens.

0022-328X/93/$6.00

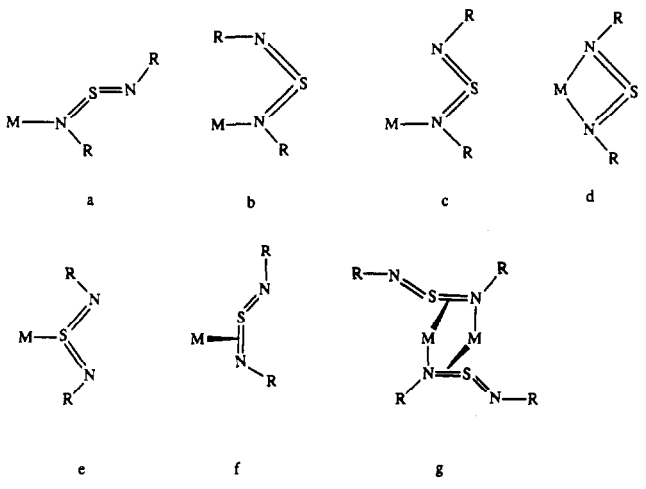

Fig. 1. Established bonding modes for sulfurdiimines.

to Pt according to the NMR spectra, was converted at temperatures above 30°C into a complex in which the N=S bond had been broken [16]. A similar activation of the N=S bonds occurred during the reaction of $Fe_2(CO)_9$ with RNSNR (R = ^{t}Bu, 4-MeC_6H_4) [17]; the sulfurdiimines decomposed by N=S bond rupture into nitrene (NR), S and RN=S fragments which were captured in clusters. From these results it is tempting to conclude that η^2-coordination of sulfurdiimines to low valent transition metals does not produce stable complexes of these ligands but leads instead to rupture of one or both N=S bonds. Stable complexes would then only be expected when the sulfurdiimine can act as a monodentate or bidentate ligand by coordination via its N or S atoms.

We show below clear evidence that this is not the case by presenting the molecular structure of the first complex in which a sulfurdiimine, *viz.* ^{t}BuN=S=N^{t}Bu (DBSD) is coordinated as an eight-electron donor ligand to two Mn atoms in the complex $(CO)_6Mn_2(\mu$-DBSD-*N,N':N,S,N'*). This complex was formed both thermally and photochemically from the thermally unstable complex $(CO)_8Mn_2$(DBSD-*N,N'*), which is the first metal–metal bonded complex containing a bidentate σ-N, σ-N' bonded sulfurdiimine. The molecular structure of this complex has also been established by an X-ray structure determination. Spectroscopic (IR, UV/Vis, resonance Raman) data are presented for the complexes $M(CO)_3Br$(DBSD-*N,N'*) (M = Mn, Re), which are the precursors of the metal–metal bonded complexes. The following equations depict the way in which the complexes under study are derived from each other.

$$M(CO)_5Br + DBSD \rightarrow M(CO)_3Br(DBSD\text{-}N,N') + 2\,CO$$

$$M(CO)_3Br(DBSD\text{-}N,N') + M'(CO)_5^- \rightarrow (CO)_8MM'(DBSD\text{-}N,N') + Br^-$$

$$(CO)_8MM'(DBSD\text{-}N,N') \rightarrow (CO)_6MM'(\mu\text{-}DBSD\text{-}N,N':N,S,N') + 2\,CO$$

M,M' = Mn, Re

2. Experimental section

2.1. Preparations

All reactions were carried out under purified nitrogen by standard Schlenk techniques. All solvents were purified by distillation and kept under nitrogen. Column chromatography was performed on silica gel (60 mesh, dried and activated before use). Di-tert-butylsulfurdiimine (DBSD) was prepared by the published method [18]. Elemental analyses were carried out by the Elemental Analyses section of the Institute for Applied Chemistry, ITC/TNO, Zeist, The Netherlands.

2.1.1. *$M(CO)_3Br(DBSD\text{-}N,N')$ (M = Mn or Re) (1a–b)*

These complexes were obtained in good yield (80–90%) by reaction of $M(CO)_5Br$ with DBSD in refluxing THF for 4–5 h. They were purified by column chromatography with hexane and then hexane/THF (3 : 1), as eluents. The first eluent was used to remove the unchanged parent compounds from the reaction product, and the desired complexes eluted with the hexane/THF mixture. The rhenium complex was red-orange and the manganese complex purple-red. *Anal.* $Mn(CO)_3Br$(DBSD-*N,N'*): C, 33.67(33.60); H, 4.73(4.61); N, 6.87(7.12). $Re(CO)_3Br$(DBSD-*N,N'*): C, 25.37(25.19); H, 3.57(3.46); N, 5.31(5.34).

2.1.2. *$(CO)_8MM'$(DBSD-N,N') (M,M = Mn, Re) (2a–d)*

The $M(CO)_5^-$ anion was obtained by reduction of $M_2(CO)_{10}$ in THF with sodium/potassium alloy. After filtration the solution of the anion was cooled to −30°C and added to a −30°C solution of the $M'(CO)_3Br$ (DBSD-*N,N'*) complex in THF. Because of the high photolability of $Mn(CO)_3Br$(DBSD-*N,N'*) and of the products, light was excluded during the reaction by wrapping the Schlenk-flask in aluminium foil. The products were purified by column chromatography at ambient temperature with exclusion of light and collection at −30°C. $(CO)_8MnRe$(DBSD-*N,N'*) (red) and $(CO)_8Mn_2$(DBSD-*N,N'*) (deep blue) were eluted with hexane, $(CO)_8ReMn$(DBSD-*N,N'*) (deep purple) with hexane/THF (1 : 1) and $(CO)_8Re_2$(DBSD-*N,N'*) (deep red) with hexane/THF (1 : 1). Owing to the thermal

instability and air sensitivity of the complexes analytical data could not be obtained. The complexes were characterized by their IR CO-stretching frequencies and by the X-ray study of $(CO)_8Mn_2$(DBSD-*N*,*N'*). For this purpose dark blue crystals of this compound were obtained by dissolving the complex in pentane and storing the solution overnight at −80°C in the dark.

2.1.3. $(CO)_6Mn_2$(μ-DBSD-N,N':N,S,N') (3)

This complex was obtained by warming a −30° solution of $(CO)_8Mn_2$(DBSD-*N*,*N'*) in hexane to room temperature with exclusion of light. The initially dark blue solution turned orange. Single crystals were obtained by cooling the hexane solution to −30° and storing it overnight at this temperature. FD-mass spectrometry gave a m/z value for the parent ion of 451.96 (calculated: 452) based on ^{57}Fe.

2.2. Spectroscopic measurements and photochemistry

IR spectra were recorded on a Nicolet 7199 B FTIR spectrophotometer with a liquid nitrogen-cooled MCT detector (32 scans, resolution 1.0 cm^{-1}) and on a Perkin-Elmer 283 spectrophotometer. ^{1}H-NMR spectra were recorded on a Bruker AMX 300 spectrometer and UV/Vis spectra on a Perkin-Elmer Lambda 5 spectrophotometer. Resonance Raman spectra of $Re(CO)_3Br$(DBSD-*N*,*N'*) (**1b**) were recorded on a Dilor XY spectrophotometer with the complex in a KNO_3 disc. The complex was excited with light from a SP 2016 argon-ion laser and a Coherent CR 590 dye laser with Coumarin 6 as a dye. The photochemistry of the complex $(CO)_8Mn_2$(DBSD-*N*,*N'*) (**2a**) was studied by irradiation of a 180 K hexane solution of this complex in a low temperature cell with the 514.5 nm laser line of a SP 2025 argon-ion laser and monitoring of the infrared spectral changes during the reaction.

2.3. Crystal structure determination of $(CO)_8Mn_2$ (DBSD-N,N') (2a)

Experimental details of the crystal structure determination of **2a** are listed in Table 1. Diffraction data were collected on an Enraf-Nonius CAD4 diffractometer using graphite-monochromated Cu Kα radiation and θ–2θ scan. The maximum value of $(\sin\theta)/\lambda$ was 0.59 $Å^{-1}$. Two reference reflections (0.20, $\bar{3}$11) were measured hourly and showed an 8% decrease during the 85 h collection time, and correction was made for this. Unit-cell parameters were refined by a least-squares fitting procedure using 23 reflections with $79 < 2\theta < 82°$. Corrections were made for Lorentz and

TABLE 1. Crystallographic data and refinement details

	2a	**3**
formula	$C_{16}H_{18}N_2O_8SMn_2$	$C_{14}H_{18}N_2O_6SMn_2$
M_r	508	452.3
cryst class	monoclinic	monoclinic
space group	$P2_1/n$	$P2_1/n$
a/Å	15.520(1)	9.2748(8)
b/Å	10.402(1)	15.145(1)
c/Å	27.207(3)	14.0433(9)
β/deg	91.869(7)	93.156(6)
V/Å^3	4389.9(8)	1969(3)
F(000)	2064	920
D_x/g cm^{-3}	1.54	1.53
Z	8	4
cryst size/mm	0.30 × 0.50 × 0.60	0.05 × 0.40 × 0.50
radiation	Cu Kα	Cu Kα
θ range/deg	2.5–65.5	2.5–70
data set	h, −18 → 0; k, 0 → 12; l, −31 → 31	h, 0 → 11; k, 0 → 18; l, −17 → 17
no. of collcd reflcns.	7458	3716
no. of obsd reflcns.	4754 ($I > 2.5\sigma(I)$)	2837 ($I > 2.5\sigma(I)$)
abs cor	applied [a]	applied [b]
non H-atoms	anisotropic	anisotropic
H atoms	isotropic	isotropic
w [c]	$1/[9.0 + F_o + 0.0068\,F_o^2]$	$1/[8.9 + F_o + 0.079F_o^2]$
R	0.068	0.050
R_w	0.099	0.068

[a] An empirical absorption correction (DIFABS, ref. 19) was applied, with coefficients in the range of 0.78–2.48. [b] The same absorption correction with coefficients in the range of 0.56–1.80. [c] F_o = observed structure factor value.

polarization effects. The positions of Mn and S were found by Direct Methods. The remainder of the non-hydrogen atoms were found in a subsequent ΔF synthesis. The hydrogen atoms were placed in calculated positions. Full-matrix least-squares refinement on F converged to $R = 0.068$, $R_w = 0.099$, $(\Delta/\sigma)_{max} = 0.20$ (C6B showed very high anisotropicity and was therefore refined isotropically). The secondary isotropic extinction coefficient [20,21] refined to $g = 0.10(2)$. A final difference Fourier map revealed a residual electron density between -0.7 and 1.6 e Å^{-3} (the maximum occurred in the vicinity of C6B). Scattering factors were taken from [22]. The anomalous scattering of Mn and S was taken into account. The X-ray data showed the presence of two types of complexes (**A** and **B**), which, however, hardly differed in bond lengths and angles. All calculations were performed with XTAL [23], unless otherwise stated. The final positional parameters and the equivalent isotropic thermal parameters for the non-hydrogen atoms are given in Table 2. Selected bond distances and angles of both complexes **2a(A)** and **2a(B)** are listed in Table 3.

2.4. Crystal structure determination of $(CO)_6Mn_2(\mu$-DBSD-N,N':N,S,N') (3)

The experimental details are listed in Table 1. The collection of diffraction data and structure determination were as described for **2a**. The maximum value of $(\sin\theta)/\lambda$ was 0.61 Å^{-1}. Two reference reflections (110,11$\bar{3}$) were measured hourly and showed no significant decrease. Unit-cell parameters were refined by a least-squares fitting procedure using 23 reflections with $80 < 2\theta < 88°$. Full-matrix least-squares refinement on F (the hydrogen atoms were restrained in such a way that the distance to their carrier carbon atom remained constant at approximately 1.09 Å) converged to $R = 0.050$, $R_w = 0.068$, $(\Delta/\sigma)_{max} = 0.36$. The secondary isotropic extinction coefficient refined to $g = 2.6(4) \times 10^2$ [20,21]. A final difference Fourier map revealed a residual electron density between -0.7 and 0.6 e Å^{-3}. The final positional parameters and the equivalent isotropic thermal parameters of the non-hydrogen atoms are given in Table 2. Selected bond distances and angles of **3** are listed in Table 4.

Supplementary data for both compounds have been deposited at the Cambridge Crystallographic Data Centre.

3. Results and discussion

3.1. $M(CO)_3Br$(DBSD-N,N') (M = Mn (1a) or Re (1b))

These complexes were prepared rather easily in high yield. They have intense colours similar to those of the corresponding M(CO)$_4$(DBSD-*N,N'*) (M = Cr, Mo, W) complexes [14]. They should in principle exist in two isomeric forms, *fac-* and *mer-*, although the *fac*-conformation of M(CO)$_3$BrL complexes has been shown to be thermodynamically much more stable when L is a chelate ligand with nitrogen donor atoms [24–27]. Normally, the two isomeric forms can easily be distinguished by IR and NMR spectroscopy. The three CO-stretching vibrations of the *fac*-form show up as three strong IR bands, the *mer*-form gives one weak and two strong CO bands [28–32]; the weak band is highest in frequency and belongs to the symmetrical stretching mode of the carbonyls *trans* to each other. The two complexes under investigation show the typical CO band pattern of the *fac*-isomer (Table 5). The CO-stretching frequencies of complexes **1a** and **1b** are in good agreement with those of the complexes M(CO)$_3$BrL in which L represents an electron withdrawing ^{t}Bu-1,4-diaza-1,3-butadiene (^{t}Bu-DAB) ligand (Table 5). This means that there is appreciable π-backbonding from both metals to the DBSD ligand. It is noteworthy, however, that this π-backbonding, contrary to the R-DAB complexes, is not reflected in a frequency decrease of ν_s(NSN) with respect to the free ligand. For free DBSD this vibration has a frequency of 1066 cm^{-1} [14], and for complex **1b** it is observed as a strong Raman band at 1113 cm^{-1} (*vide infra*). Similar behaviour has, however, been observed for the complexes M(CO)$_4$(DBSD-*N,N'*) (M = Cr, Mo, W), which show ν_s(NSN) at 1070–1090 cm^{-1} [14]. Probably the frequency of this vibration is influenced not only by σ-donation and π-backbonding effects but also by the rather drastic structural change of the ligand on going from the free *cis, trans*-conformation to the chelate bonded *trans, trans*-configuration with a much smaller NSN angle. This is evident, for example, from the behaviour of ν_s(NSN) going from free D^{i}PrSD (^{i}Pr = *iso*-propyl) (1056 cm^{-1}) to W(CO)$_5$(D^{i}PrSD-*N*) (1023 cm^{-1}) and Cr(CO)$_4$(D^{i}PrSD-*N,N'*) (1095 cm^{-1}) [14]. In the complex W(CO)$_5$(D^{i}PrSD-*N*) the ligand has retained its *cis, trans*-conformation and coordination causes a lowering of frequency for ν_s(NSN). When a chelate is formed in Cr(CO)$_4$(DiPrSD-*N,N'*), this frequency increases again, although π-backbonding is stronger in this tetracarbonyl complex. The same *fac*-conformation of the complexes is indicated by the ^{1}H-NMR spectra, which show only one signal for the ^{t}Bu protons (Table 5). Relative to the free ligand there is an expected shift to lower field for both complexes.

The electronic absorption spectra of **1** are characterized by strong bands in the visible region (Table 5, Fig. 2). Both the intensities of these bands and their solvent dependence (see Table 5) point to an assignment in terms of metal to DBSD charge transfer (MLCT) transitions. Similar MLCT bands were observed previously

for the corresponding $M(CO)_4$(DBSD-*N*,*N'*) (M = Cr, Mo, W) complexes, but in that case the bands were only solvatochromic for M = Cr and Mo [14]. The complexes under study differ in the appearance of their visible band in that it is structured for the Re-complex (**1b**) but highly symmetric for the Mn-complex (**1a**) (Fig. 2) just as for $M(CO)_4$(DBSD-*N*,*N'*) [14]. Such a structured band points to the presence of at least two MLCT transitions from different metal orbitals. In fact, of the three symmetry-allowed MLCT transitions, only two will be intense since the third transition is overlap forbidden. From the remaining two transitions, the most intense one will be that between the Re(d_π) and DBSD(π^*) orbitals having the same a' symmetry and giving rise to the strong metal-to-DBSD π-backbonding. The interaction between the filled metal and bromide (p_π) orbitals may also be of importance and influence the characters of the highest filled orbitals and lowest energy transitions. We have previously, for example, demonstrated halide character for an electronic transition of the complex $Re(CO)_3Br$(p-Tol-DAB-*N*,*N'*) [33] and very recently for the complexes Ru(X)(R)$(CO)_2$(α-diimine-*N*,*N'*) (X = halide, R = alkyl) [34].

In order to gain more information about the characters of these electronic transitions we have studied the resonance Raman (rR) spectra of complex **1b**. Complex **1a** was too photolabile for such a rR study. Preliminary rR measurements of the complex in CH_2Cl_2 gave rather poor results. Better spectra were obtained by incorporating the complex into a KNO_3 disc. The $\nu_s(NO_3^-)$ Raman band at 1051 cm^{-1} was used as internal standard. Two representative spectra, one excited at the low-energy side of the absorption band (λ_{exc} = 536 nm), the other close to its maximum (λ_{exc} = 458 nm), are presented in Fig. 3.

Resonance enhancement of Raman intensity is observed for bands at 193, 228, 438, 476, 497, 618, 781, 855, 1113, 1210 and 2015 cm^{-1}. The spectra in Fig. 3 show that the two electronic transitions within the absorption band give rise to different rR effects, although more or less the same vibrations are involved in the vibronic coupling. The 193 cm^{-1} band belongs to ν(Re–Br); for the corresponding complex $Re(CO)_3Br$ (pTol-DAB-*N*,*N'*) it was recently observed at 190 cm^{-1} [33]. The band at 228 cm^{-1} is assigned to ν_s(Re–N); the corresponding ν_s(W–N) vibration of $W(CO)_4$-(DBSD-*N*,*N'*) has been observed at the same frequency [14,35]. The bands at 476 and 497 cm^{-1} belong to ν_s(Re–C) vibrations. They have wavenumbers similar to those for the corresponding $W(CO)_4$(DBSD-*N*,*N'*) [14,35] and $Re(CO)_3X$(R-DAB-*N*,*N'*) (X = halide) complexes [36]. The Raman band at 438 cm^{-1} shows a similar, strong, rR effect to those of the bands at 781 and 855 cm^{-1}. All three bands are assigned to deformation modes of the DBSD ligand (*vide infra*). The 618 cm^{-1} band certainly belongs to a δ(ReCO) vibration and the bands at 1113 and 1210 cm^{-1} to ν_s(NSN) and ν_{as}(NSN) of the DBSD ligand, respectively. For the free DBSD ligand these symmetric and antisymmetric stretching vibrations are found at 1066 and 1194 cm^{-1}, respectively [14,18]. The 2015 cm^{-1} band belongs to one of the two symmetrical stretching modes of the carbonyls (= ν_s(CO)). According to the Raman spectra both ν_s(Re–N) at 228 cm^{-1} and ν_s(NSN) at 1113 cm^{-1} are vibronically coupled to the electronic transitions in agreement with their MLCT character. However, the rR effect of ν_s(NSN) is stronger for the second transition, which means that this transition has more MLCT character. At the same time both ν(Re–Br) at 193 cm^{-1} and ν_s(CO) at 2015 cm^{-1} show a much stronger rR effect upon excitation into this higher-energy transition.

From these observations we suggest that the first transition, giving rise to the long-wavelength shoulder of the visible band, is between the Re(d_π) and DBSD (π^*) orbitals having the same symmetry and responsible for the metal to ligand π-backbonding. Charge transfer is lowest for this $a'(d_\pi) \rightarrow a'(\pi^*)$ transition, and as a result the rR effects for ν(Re–Br) and ν_s(CO) are only weak. The $a''(d_\pi) \rightarrow a'(\pi^*)$ transition has more MLCT character, and is therefore accompanied by stronger rR effects for ν(Re–Br) and ν_s(CO). Although rather strong rR effects are observed for ν_s(Re–N) throughout the absorption band, this effect is more pronounced for the second transition. Apparently, this transition more strongly affects the metal–nitrogen bonds. In addition, strong rR effects are observed for Raman bands at 438, 781 and 855 cm^{-1} and a weaker effect for ν_{as}(NSN) at 1210 cm^{-1}. Free DBSD has a deformation mode (δ(NSN)), at 678 cm^{-1}, which increases in frequency upon coordination as a chelate [14]. Probably the 781 and 855 cm^{-1} bands belong to such deformation modes, and the MLCT transitions are accompanied by in-plane distortions of the DBSD ligand.

Similar rR effects have been observed for ligand deformation modes in the region 500–900 cm^{-1} in the case of α-diimine complexes [6,36]. If the complex retains its ground-state symmetry upon excitation, rR effects for an antisymmetric vibration such as ν_{as}(NSN) will not be observed, and so the appearance of this vibration in the rR spectra indicates that the complex loses its C_s symmetry upon excitation because of an asymmetric distortion of the DBSD ligand. The Raman band at 438 cm^{-1} most probably belongs to an out-of-plane deformation mode of DBSD. The observation of a strong rR effect for this vibration points to an out-

of-plane distortion of the ligand, which is apparently stronger for the first transition. It is noteworthy that this 438 cm^{-1} band is not present as a strong rR band in the spectra of the corresponding $W(CO)_4$(DBSD-*N,N'*) complex. This difference in behaviour is probably due to the presence of axial Br^- and CO ligands instead of two carbonyls. The repulsive interaction between the negative charges at the DBSD ligand and Br^- in the MLCT excited states may cause an out-of-plane distortion of DBSD away from the Br^- ligand.

3.2. $(CO)_8MM'$(DBSD-N,N') (M,M' = Mn, Re) (2a–d)

The notation used for the complexes is explained in Table 5. Complexes **2** exhibit rather complicated IR spectra in the CO stretching region but these are in reasonably good agreement with those for the corresponding α-diimine complexes $(CO)_8MM'$(α-diimine-*N,N'*) [6] (Table 5). On going from the mononuclear to the binuclear complexes the visible absorption band shifts to longer wavelength (Table 5, Fig. 2). This behaviour, which has also been observed for the corresponding α-diimine complexes [6], is consistent with the MLCT character of these bands and reflects the higher electron density at the central metal atom in the case of **2**.

3.2.1. Crystal structure of 2a

The crystal structure has been determined for one of these complexes, $(CO)_8Mn_2$(DBSD-*N,N'*) (**2a**). ORTEP and PLUTO [37] drawings are shown in Fig. 4, and the crystallographic data are listed in Tables 1–3. Bond lengths and angles are given for only one of the two independent molecules in the unit cell. Both Mn atoms possess a distorted octahedral geometry. The Mn–Mn distance of 2.967 Å is somewhat longer than that in $Mn_2(CO)_{10}$ (2.9038 Å) [38]. The Mn–CO distances in the equatorial plane of the $Mn(CO)_5$ moiety are very similar (1.84–1.87 Å), but somewhat longer than the bond distance between Mn(2) and the axial C(13)O(13) ligand (1.78 Å). This effect is due to the stronger competition between the equatorial carbonyls with respect to the π-backbonding interaction with Mn(2). The high π-electron density in the axial Mn(2)–C(13) bond may also be responsible for the bending of the equatorial carbonyls towards the $Mn(CO)_3$(DBSD-*N,N'*) moiety. Similar effects have been observed for the complex $(CO)_8ReMn(^iPr\text{-}DAB\text{-}N,N')$ [39].

The two carbonyls in the equatorial plane of the $Mn(CO)_3$(DBSD-*N,N'*) fragment (C(9)O(9) and C(10)O(10)) are in a staggered position with respect to the equatorial carbonyls of the $Mn(CO)_5$ group. The same conformation has been found for $Mn_2(CO)_{10}$ [38] and $(CO)_8ReMn(^iPr\text{-}DAB\text{-}N,N')$ [39]. The two Mn–CO distances in the equatorial plane of the $Mn(CO)_3$(DBSD-*N,N'*) group are shorter (1.78–1.80 Å) than those for the corresponding carbonyls in the $Mn(CO)_5$ part (1.84–1.87 Å). There is, apparently, less competition between these carbonyls and the DBSD ligand in respect of the π-backbonding interaction with Mn(1). All three Mn–CO bond lengths in this fragment are now nearly equal, and similar to the Mn(2)–C(13)–O(13) bond length. There is, however, a repulsive interaction between DBSD and the axial C(11)O(11) ligand, since the Mn(2)–Mn(1)–C(11) angle is only 161.7°. The DBSD ligand, which is bonded as a chelate to the metal has a structure similar to that in $W(CO)_4$(DBSD-*N,N'*) [40]. In both complexes the ligand has a *trans, trans*-conformation and the N–S bond lengths and NSN bond angle are nearly the same. For comparison these latter data are presented in Table 6, together with those for the free ligands di-p,p'-tolylsulfurdiimine (DTSD) [41] and dimethylsulfurdiimine (DMSD) [42] and the complex *trans*-$PtCl_2(C_2H_4)$(DBSD-*N*) [43], in which the sulfurdiimine is coordinated as a monodentate ligand.

The NS bonds of DBSD in **2a** and $W(CO)_4$(DBSD-*N,N'*) have retained their double bond character since they are only slightly elongated with respect to the free molecule. This also explains why ν_s(NSN) of $W(CO)_4$(DBSD-*N,N'*) [14] and **1b** (*vide supra*) are only slightly shifted in frequency with respect to the free ligand. For **2a** the frequency of this vibration could not be determined by rR spectroscopy because of the high photolability of this complex (*vide infra*). The NSN angle has changed dramatically upon coordination of the ligand in $W(CO)_4$(DBSD-*N,N'*) and **2a**; relative to those for free DTSD and DMSD and the Pt-complex it has decreased by about 20°. This change of bond angle is also reflected in the high-frequency shift of the NSN deformation modes of $W(CO)_4$(DBSD-*N,N'*) and **1b** with respect to free DBSD.

3.3. Thermal and photochemical conversion of 2a into 3

All the complexes **2** are photolabile and also thermally labile under ambient conditions. Because of this instability the thermal and photochemical reactions were studied only for one representative complex, **2a**. When the temperature of a solution of **2a** in n-hexane was raised to room temperature the absorption band at 577 nm disappeared, and a new band appeared at 410 nm. During this process the colour of the solution changed from deep blue to orange. At the same time new CO IR bands appeared that had similar frequencies as those of $(CO)_6Mn_2$(μ-R-DAB-*N,N':N,C,C',N'*) (R = ^{i}Pr, ^{p}Tol) [44] (Table 5), in which the R-DAB ligand is σ,σ-coordinated to one Mn atom and η^4 to

TABLE 2. Fractional coordinates of the non-hydrogen atoms with esd's in parentheses and the equivalent isotropic thermal parameters for **2a** (**A** and **B**) and **3**

	x	y	z	U_{eq}
2a (A)				
Mn(1A)	0.52842(7)	0.2675(1)	0.76760(4)	0.0246(6)
Mn(2A)	0.41496(8)	0.0622(1)	0.72616(5)	0.0310(7)
S(1A)	0.5870(1)	0.3931(2)	0.68635(7)	0.032(1)
C(1A)	0.7054(5)	0.2151(8)	0.7023(3)	0.033(4)
C(2A)	0.7440(7)	0.152(2)	0.7479(5)	0.10(1)
C(3)	0.6889(7)	0.117(1)	0.6622(5)	0.10(1)
C(4A)	0.7658(6)	0.316(1)	0.6835(5)	0.10(1)
C(5A)	0.4516(6)	0.5285(8)	0.7105(3)	0.036(5)
C(6A)	0.3548(6)	0.4869(9)	0.7064(4)	0.051(6)
C(7A)	0.4636(6)	0.6115(9)	0.7574(3)	0.045(5)
C(8A)	0.4756(7)	0.6029(9)	0.6656(4)	0.057(7)
C(9A)	0.5630(5)	0.1314(9)	0.8037(3)	0.034(5)
C(10A)	0.4351(5)	0.2837(9)	0.8051(3)	0.037(5)
C(11A)	0.5857(6)	0.3685(9)	0.8102(3)	0.039(5)
C(12A)	0.4542(5)	0.1501(9)	0.6725(3)	0.035(5)
C(13)	0.3548(6)	−0.565(9)	0.6917(4)	0.044(5)
C(14A)	0.5106(6)	−0.043(1)	0.7265(4)	0.050(6)
C(15A)	0.3191(6)	0.1700(9)	0.7299(3)	0.039(5)
C(16A)	0.3919(6)	0.003(1)	0.7880(4)	0.051(6)
N(1A)	0.6219(4)	0.2711(7)	0.7165(2)	0.027(3)
N(2A)	0.5031(4)	0.4089(7)	0.7184(3)	0.033(4)
O(9A)	0.5868(4)	0.0510(7)	0.8302(2)	0.055(4)
O(10A)	0.3801(4)	0.3026(8)	0.8314(2)	0.058(4)
O(11A)	0.6207(5)	0.4345(8)	0.8389(3)	0.065(5)
O(12A)	0.4733(4)	0,1979(7)	0.6373(2)	0.044(4)
O(13)	0.3163(5)	−0.1317(7)	0.6693(3)	0.064(4)
O(14A)	0.5670(5)	−0.1102(8)	0.7254(3)	0.074(6)
O(15A)	0.2585(4)	0.2285(7)	0.7316(3)	0.056(4)
O(16A)	0.3772(6)	−0.035(1)	0.8265(3)	0.088(6)
2a (B)				
Mn(1B)	0.21291(8)	0.2542(1)	0.47305(4)	0.0271(7)
Mn(2B)	0.39894(8)	0.2248(1)	0.49851(5)	0.0330(7)
S(1B)	0.1496(1)	0.3741(2)	0.55415(7)	0.036(7)
C(1B)	0.1266(6)	0.1302(9)	0.5741(3)	0.040(5)
C(2B)	0.1318(9)	0.000(1)	0.5496(5)	0.09(1)
C(3B)	0.1862(8)	0.124(1)	0.6210(4)	0.073(8)
C(4B)	0.0382(7)	0.163(1)	0.5901(5)	0.09(1)
C(5B)	0.1894(7)	0.5676(9)	0.4973(4)	0.050(6)
C(6B)	0.206(6)	0.594(2)	0.4435(9)	0.19(1)
C(7B)	0.266(1)	0.621(2)	0.5169(9)	0.30(4)
C(8B)	0.115(1)	0.631(1)	0.5156(7)	0.16(2)
C(9B)	0.2291(6)	0.0896(9)	0.4558(3)	0.038(5)
C(10B)	0.2609(5)	0.307(1)	0.4168(3)	0.040(5)
C(11B)	0.1111(6)	0.2489(9)	0.4413(3)	0.038(5)
C(12B)	0.3536(6)	0.310(1)	0.5511(3)	0.041(5)
C(13B)	0.5018(6)	0.214(1)	0.5237(3)	0.044(6)
C(14B)	0.3728(6)	0.0729(9)	0.5283(3)	0.042(5)
C(15B)	0.4234(6)	0.380(1)	0.4678(3)	0.042(5)
C(16B)	0.4192(6)	0.412(1)	0.4397(4)	0.046(6)
N(1B)	0.1629(4)	0.2276(6)	0.5399(2)	0.030(4)
N(2B)	0.1916(4)	0.4275(7)	0.5053(2)	0.034(4)
O(9B)	0.2350(5)	−0.0162(7)	0.4438(3)	0.060(5)
O(10B)	0.2859(4)	0.3390(9)	0.3790(2)	0.061(5)
O(11B)	0.0451(4)	0.2431(8)	0.4204(3)	0.059(5)
O(12B)	0.3338(5)	0.3668(8)	0.5856(2)	0.060(5)
O(13B)	0.5757(4)	0.2074(8)	0.5403(3)	0.058(5)
O(14B)	0.3617(5)	−0.0242(8)	0.5473(3)	0.071(5)
O(15B)	0.4420(5)	0.4730(8)	0.4492(3)	0.062(5)
O(16B)	0.4349(5)	0.0938(8)	0.4034(3)	0.068(5)

TABLE 2 (*continued*)

	x	y	z	U_{eq}
3				
Mn(1)	0.54991(8)	0.69752(5)	0.15518(5)	0.0389(4)
Mn(2)	0.71437(8)	0.67030(5)	0.29806(5)	0.387(4)
S	0.7196(1)	0.54844(7)	0.21087(9)	0.0434(6)
C(1)	0.3886(7)	0.7483(4)	0.1945(4)	0.061(3)
C(2)	0.5821(6)	0.8015(4)	0.0965(4)	0.060(3)
C(3)	0.4525(7)	0.6561(4)	0.0532(4)	0.059(3)
C(4)	0.9240(6)	0.7074(4)	0.3225(4)	0.057(3)
C(5)	0.6730(6)	0.7794(4)	0.3152(4)	0.056(3)
C(6)	0.7356(6)	0.6464(4)	0.4245(4)	0.057(3)
C(7)	0.4630(6)	0.5367(3)	0.2938(4)	0.048(3)
C(8)	0.5437(8)	0.4652(4)	0.3511(5)	0.071(4)
C(9)	0.3753(8)	0.5925(5)	0.3583(5)	0.070(4)
C(10)	0.3658(8)	0.4939(5)	0.2144(5)	0.076(4)
C(11)	0.8659(6)	0.6451(3)	0.0851(3)	0.046(3)
C(12)	0.9904(7)	0.5872(5)	0.1220(5)	0.067(4)
C(13)	0.8029(8)	0.6111(6)	−0.0107(4)	0.073(4)
C(14)	0.9175(8)	0.7396(4)	0.0765(6)	0.071(4)
N(1)	0.5664(4)	0.5957(2)	0.2450(3)	0.039(2)
N(2)	0.7458(4)	0.6456(2)	0.1526(3)	0.036(2)
O(1)	0.2863(6)	0.7843(4)	0.2156(4)	0.098(4)
O(2)	0.5989(6)	0.8682(3)	0.0607(4)	0.099(4)
O(3)	0.3885(6)	0.6263(4)	−0.0118(3)	0.098(4)
O(4)	1.0348(5)	0.7328(4)	0.3417(3)	0.098(4)
O(5)	0.6321(6)	0.8494(3)	0.3343(4)	0.085(3)
O(6)	0.7373(6)	0.6340(4)	0.5039(3)	0.094(4)

the other. Accordingly this new product (**3**) was tentatively formulated as $(CO)_6Mn_2$(μ-DBSD-*N,N':N,S,N'*). This structure was confirmed by an X-ray determination of complex **3** (*vide infra*).

The thermal formation of **3** from **2a** might in principle occur by loss of CO from the $Mn(CO)_5$ moiety or by homolysis of the Mn–Mn bond followed by a reaction between the $Mn(CO)_5$ and $Mn(CO)_3$(DBSD-*N,N'*) radicals formed. The latter mechanism has been established for the photochemical formation of $(CO)_6Mn_2$ (μ-R-DAB-*N,N':N,C,C',N'*) complexes out of $(CO)_8Mn_2$(R-DAB-*N,N'*) [44]. In the latter case, however, there was only complete conversion into this product when the reaction was performed in a very viscous solvent, such as paraffin, in which the $Mn(CO)_5$ radicals could hardly diffuse. In less viscous media $Mn_2(CO)_{10}$ and $(CO)_6Mn_2$(R-DAB-*N,N'*)$_2$ were instead formed as the main products. The thermal conversion of **2a** into **3** was not accompanied by formation of $Mn_2(CO)_{10}$, which points to loss of CO from the intact metal–metal bonded complex as primary process. This conclusion seems to be in conflict with the observation that, when the temperature of a solution of **2a** was raised in the presence of CBr_4, $Mn(CO)_5Br$ was formed as the only detectable product. Carbon tetrabromide is known to be a good scavenger of radicals and $Mn(CO)_5Br$ is therefore expected to be formed by reaction of this compound with $Mn(CO)_5$ radicals. It is possible that $Mn(CO)_5Br$ is formed by reaction of CBr_4

TABLE 3. Selected bond distances (Å) and angles (deg) in **2a** (**A** and **B**) with esd's in parentheses

Mn(1A)–Mn(2A)	2.967(2)	Mn(1B)–Mn(2B)	2.936(2)
Mn(1A)–C(9A)	1.795(9)	Mn(1B)–C(9B)	1.80(1)
Mn(1A)–C(10A)	1.805(8)	Mn(1B)–C(10B)	1.810(9)
Mn(1A)–C(11A)	1.781(9)	Mn(1B)–C(11B)	1.7779(9)
Mn(1A)–N(1A)	2.042(6)	Mn(1B)–N(1B)	2.020(7)
Mn(1A)–N(2A)	2.018(7)	Mn(1B)–N(2B)	2.037(7)
Mn(2A)–C(12A)	1.841(9)	Mn(2B)–C(12B)	1.843(9)
Mn(2A)–C(13A)	1.79(1)	Mn(2B)–C(13B)	1.809(9)
Mn(2A)–C(14A)	1.84(1)	Mn(2B)–C(14B)	1.83(1)
Mn(2A)–C(15A)	1.87(1)	Mn(2B)–C(15B)	1.86(1)
Mn(2A)–C(16A)	1.84(1)	Mn(2B)–C(16B)	1.85(1)
S(1A)–N(1A)	1.595(7)	S(1B)–N(1B)	1.587(7)
S(1A)–N(2A)	1.599(7)	S(1B)–N(2B)	1.599(7)
C(9A)–O(9A)	1.16(1)	C(9B)–O(9B)	1.15(1)
C(10A)–O(10A)	1.15(1)	C(10B)–O(10B)	1.16(1)
C(11A)–O(11A)	1.16(1)	C(11B)–O(11B)	1.16(1)
C(12A)–O(12A)	1.13(1)	C(12B)–O(12B)	1.16(1)
C(13A)–O(13A)	1.15(1)	C(13B)–O(13B)	1.13(1)
C(14A)–O(14A)	1.12(1)	C(14B)–O(14B)	1.15(1)
C(15A)–O(15A)	1.12(1)	C(15B)–O(15B)	1.13(1)
C(16A)–O(16A)	1.15(1)	C(16B)–O(16B)	1.14(1)
Mn(2A)–Mn(1A)–C(9A)	78.7(3)	Mn(2B)–Mn(1B)–C(9B)	79.6(3)
Mn(2A)–Mn(1A)–C(10A)	78.7(3)	Mn(2B)–Mn(1B)–C(10B)	78.7(3)
Mn(2A)–Mn(1A)–C(11A)	161.7(3)	Mn(2B)–Mn(1B)–C(11B)	162.8(3)
Mn(2A)–Mn(1A)–N(1A)	100.4(2)	Mn(2B)–Mn(1B)–N(1B)	100.1(2)
Mn(2A)–Mn(1A)–N(2A)	99.9(2)	Mn(2B)–Mn(1B)–N(2B)	99.3(2)
C(9A)–Mn(1A)–C(10A)	89.7(4)	C(9B)–Mn(1B)–C(10B)	90.3(4)
C(9A)–Mn(1A)–C(11A)	88.6(4)	C(9B)–Mn(1B)–C(11B)	88.5(4)
C(9A)–Mn(1A)–N(1A)	100.4(3)	C(9B)–Mn(1B)–N(1B)	99.5(3)
C(9A)–Mn(1A)–N(2A)	170.2(3)	C(9B)–Mn(1B)–N(2B)	169.4(3)
C(10A)–Mn(1A)–C(11A)	88.3(4)	C(10B)–Mn(1B)–C(11B)	89.0(4)
C(10A)–Mn(1A)–N(1A)	169.5(3)	C(10B)–Mn(1B)–N(1B)	169.8(4)
C(10A)–Mn(1A)–N(2A)	99.5(4)	C(10B)–Mn(1B)–N(2B)	99.9(4)
C(11A)–Mn(1A)–N(1A)	94.7(3)	C(11B)–Mn(1B)–N(1B)	94.1(3)
C(11A)–Mn(1A)–N(2A)	94.9(4)	C(11B)–Mn(1B)–N(2B)	94.7(4)
N(1A)–Mn(1A)–N(2A)	70.2(3)	N(1B)–Mn(1B)–N(2B)	70.2(3)
Mn(1A)–Mn(2A)–C(12A)	74.7(3)	Mn(1B)–Mn(2B)–C(12B)	74.8(3)
Mn(1A)–Mn(2A)–C(13A)	170.5(3)	Mn(1B)–Mn(2B)–C(13B)	171.0(3)
Mn(1A)–Mn(2A)–C(14A)	87.6(3)	Mn(1B)–Mn(2B)–C(14B)	88.0(3)
Mn(1A)–Mn(2A)–C(15A)	90.6(3)	Mn(1B)–Mn(2B)–C(15B)	91.0(3)
Mn(1A)–Mn(2A)–C(16A)	91.3(3)	Mn(1B)–Mn(2B)–C(16B)	92.1(3)
C(12A)–Mn(2A)–C(13A)	96.2(4)	C(12B)–Mn(2B)–C(13B)	96.4(4)
C(12A)–Mn(2A)–C(14A)	90.6(4)	C(12B)–Mn(2B)–C(14B)	88.7(4)
C(12A)–Mn(2A)–C(15A)	91.7(4)	C(12B)–Mn(2B)–C(15B)	91.1(4)
C(12A)–Mn(2A)–C(16A)	166.1(4)	C(12B)–Mn(2B)–C(16B)	166.9(4)
C(13A)–Mn(2A)–C(14A)	90.0(4)	C(13B)–Mn(2B)–C(14B)	89.9(4)
C(13A)–Mn(2A)–C(15A)	92.3(4)	C(13B)–Mn(2B)–C(15B)	91.2(4)
C(13A)–Mn(2A)–C(16A)	97.7(5)	C(13B)–Mn(2B)–C(16B)	96.6(4)
C(14A)–Mn(2A)–C(15A)	176.5(4)	C(14B)–Mn(2B)–C(15B)	178.9(4)
C(14A)–Mn(2A)–C(16A)	88.8(5)	C(14B)–Mn(2B)–C(16B)	91.7(4)
C(15A)–Mn(2A)–C(16A)	88.3(4)	C(15B)–Mn(2B)–C(16B)	88.3(4)
N(1A)–S(1A)–N(2A)	94.0(3)	N(1B)–S(1B)–N(2B)	94.1(4)
Mn(1A)–C(9A)–O(9A)	174.2(8)	Mn(1B)–C(9B)–O(9B)	174.3(8)
Mn(1A)–C(10A)–O(10A)	173.5(8)	Mn(1B)–C(10B)–O(10B)	175.0(8)
Mn(1A)–C(11A)–O(11A)	177.8(8)	Mn(1B)–C(11B)–O(11B)	178.7(9)
Mn(2A)–C(12A)–O(12A)	174.1(8)	Mn(2B)–C(12B)–O(12B)	172.9(8)
Mn(2A)–C(13)–O(13A)	179.4(9)	Mn(2B)–C(13B)–O(13B)	178.6(9)
Mn(2A)–C(14A)–O(14A)	177.2(9)	Mn(2B)–C(14B)–O(14B)	175.8(9)
Mn(2A)–C(15A)–O(15A)	175.8(9)	Mn(2B)–C(15B)–O(15B)	177.0(9)

TABLE 3 (*continued*)

Mn(2A)–C(16A)–O(16A)	179(1)	Mn(2B)–C(16B)–O(16B)	177.3(9)
Mn(1A)–N(1A)–S(1A)	97.4(3)	Mn(1B)–N(1B)–S(1B)	98.3(3)
Mn(1A)–N(1A)–C(1A)	144.7(5)	Mn(1B)–N(1B)–C(1B)	144.6(5)
S(1A)–N(1A)–C(1A)	117.6(5)	S(1B)–N(1B)–C(1B)	116.3(5)
Mn(1A)–N(2A)–S(1A)	98.2(3)	Mn(1B)–N(2B)–S(1B)	97.3(4)
Mn(1A)–N(2A)–C(5A)	142.6(6)	Mn(1B)–N(2B)–C(5B)	144.5(6)
S(1A)–N(2A)–C(5A)	116.8(6)	S(1B)–N(2B)–C(5B)	117.3(6)

with the undissociated complex **2a** and that this reaction is much faster than the loss of CO leading to the formation of **3**. Because of its thermal lability the photochemistry of **2a** could only be studied at low temperatures. Irradiation of a solution of the complex in n-hexane at 183 K again gave **3**, but in addition two other products were observed. The complex $Mn_2(CO)_{10}$ was formed as a side-product, and $(CO)_7Mn_2(\mu$-DBSD-$N,N':N,S)$ was observed as an intermediate in the photoconversion of **2a** into **3**. The $(CO)_7Mn_2(\mu$-DBSD-$N,N':N,S)$ species was identified as such by the close similarity between its CO stretching frequencies and those of $(CO)_7Mn_2(\mu$-^{i}Pr-PyCa-$N,N':N,C)$ (PyCa = pyridine-carbaldehyde imine) (Table 5) in which the ^{i}Pr-PyCa ligand is σ-N, σ-N′ coordinated to one Mn atom and η^2 to the other via its reactive imine (C=N) group [44]. The formation of $Mn_2(CO)_{10}$ and the close correspondence with the photoreactions of the corresponding R-PyCa and R-DAB complexes indicate that the reaction proceeds by homolysis of the metal–metal bond as the primary photoprocess. The formation of $(CO)_7Mn_2(\mu$-DBSD-$N,N':N,S)$ and $(CO)_6Mn_2(\mu$-DBSD-$N,N':N,S,N')$ (**3**) can then be explained in terms of the mechanism that we established for the photoreactions of the corresponding $(CO)_8Mn_2$(R-DAB-$N,N')$ and $(CO)_8Mn_2$(R-PyCa-$N,N')$ complexes [6,44] (Scheme 1).

TABLE 4. Selected bond distances (Å) and angles (deg) in **3** with esd's in parentheses

Mn(1)–Mn(2)	2.638(1)	Mn(2)–N(1)	2.082(4)
Mn(1)–C(1)	1.796(6)	Mn(2)–N(2)	2.080(4)
Mn(1)–C(2)	1.810(6)	S–N(1)	1.684(4)
Mn(1)–C(3)	1.766(6)	S–N(2)	1.707(4)
Mn(1)–N(1)	1.993(4)	C(1)–O(1)	1.148(8)
Mn(1)–N(2)	1.982(4)	C(2)–O(2)	1.143(8)
Mn(2)–S	2.218(1)	C(3)–O(3)	1.154(8)
Mn(2)–C(4)	1.800(6)	C(4)–O(4)	1.147(7)
Mn(2)–C(5)	1.791(6)	C(5)–O(5)	1.162(7)
Mn(2)–C(6)	1.815(5)	C(6)–O(6)	1.131(7)
Mn(2)–Mn(1)–C(1)	111.8(2)	C(5)–Mn(2)–C(6)	91.3(3)
Mn(2)–Mn(1)–C(2)	111.2(2)	C(5)–Mn(2)–N(1)	105.9(2)
Mn(2)–Mn(1)–C(3)	148.7(2)	C(5)–Mn(2)–N(2)	108.9(2)
Mn(2)–Mn(1)–N(1)	51.1(1)	C(6)–Mn(2)–N(1)	100.2(2)
Mn(2)–Mn(1)–N(2)	51.1(1)	C(6)–Mn(2)–N(2)	158.1(2)
C(1)–Mn(1)–C(2)	85.9(3)	N(1)–Mn(2)–N(2)	66.9(1)
C(1)–Mn(1)–C(3)	90.2(3)	Mn(2)–S–N(1)	62.7(1)
C(1)–Mn(1)–N(1)	100.0(2)	Mn(2)–S–N(2)	62.4(1)
C(1)–Mn(1)–N(2)	162.9(2)	N(1)–S–N(2)	85.2(2)
C(2)–Mn(1)–C(3)	91.7(3)	Mn(1)–C(1)–O(1)	176.1(6)
C(2)–Mn(1)–N(1)	162.3(2)	Mn(1)–C(2)–O(2)	177.9(6)
C(2)–Mn(1)–N(2)	99.4(2)	Mn(1)–C(3)–O(3)	177.6(6)
C(3)–Mn(1)–N(1)	104.9(2)	Mn(2)–C(4)–O(4)	176.9(5)
C(3)–Mn(1)–N(2)	105.8(2)	Mn(2)–C(5)–O(5)	174.3(5)
N(1)–Mn(1)–N(2)	70.5(2)	Mn(2)–C(6)–O(6)	176.8(6)
Mn(1)–Mn(2)–S	70.92(2)	Mn(1)–N(1)–Mn(2)	80.6(1)
Mn(1)–Mn(2)–C(4)	133.1(1)	Mn(1)–N(1)–S	100.7(2)
Mn(1)–Mn(2)–C(5)	74.3(2)	Mn(1)–N(1)–C(7)	136.0(3)
Mn(1)–Mn(2)–C(6)	136.1(2)	Mn(2)–N(1)–S	71.3(1)
Mn(1)–Mn(2)–N(1)	48.2(1)	Mn(2)–N(1)–C(7)	131.6(3)
Mn(1)–Mn(2)–N(2)	47.9(1)	S–N(1)–C(7)	116.6(3)
S–Mn(2)–C(4)	114.9(2)	Mn(1)–N(2)–Mn(2)	80.9(1)
S–Mn(2)–C(5)	145.1(2)	Mn(1)–N(2)–S	100.3(2)
S–Mn(2)–C(6)	111.5(2)	Mn(1)–N(2)–C(11)	136.6(3)
S–Mn(2)–N(1)	46.0(1)	Mn(2)–N(2)–S	70.9(1)
S–Mn(2)–N(2)	46.7(1)	Mn(2)–N(2)–C(11)	132.6(3)
C(4)–Mn(2)–C(5)	91.3(3)	S–N(2)–C(11)	115.4(3)
C(4)–Mn(2)–N(2)	100.0(2)		

According to this mechanism irradiation of **2a** leads to the formation of $Mn(CO)_5$ and $Mn(CO)_3$(DBSD-$N,N')$ radicals. At this low temperature the diffusion of the radicals is restricted and so only a small amount of $Mn_2(CO)_{10}$ is formed. Back-reaction of the $Mn(CO)_5$ and $Mn(CO)_3$(DBSD-$N,N')$ radicals to give the parent complex **2a** cannot occur by a simple metal–metal coupling reaction since the unpaired electron of the $Mn(CO)_3$(DBSD-$N,N')$ radical will mainly reside in the low-lying π^* orbital of the DBSD ligand. This radical can therefore better be formulated as $Mn^+(CO)_3$(DBSD-N,N'^-). Because of this, the $Mn(CO)_3$(DBSD-$N,N')$ radical will attack the Mn atom of the $Mn(CO)_5$ radical via its $DBSD^-$ radical anion. This reaction leads to formation of a η^2-bond between Mn and a NS bond of DBSD with loss of CO and formation of a new Mn–Mn bond. The $(CO)_7Mn_2(\mu$-DBSD-$N,N':N,S)$ complex thus formed is apparently unstable, and undergoes further loss of CO with formation of $(CO)_6Mn_2(\mu$-DBSD-$N,N':N,S,N')$. In the case of the complexes $(CO)_8Mn_2$(R-PyCa-$N,N')$ this reaction stops when $(CO)_7Mn_2(\mu$-R-PyCa-$N,N':N,C)$ is formed, since only the imine group of this ligand and not its pyridine ring will form a η^2-bond. In the R-DAB

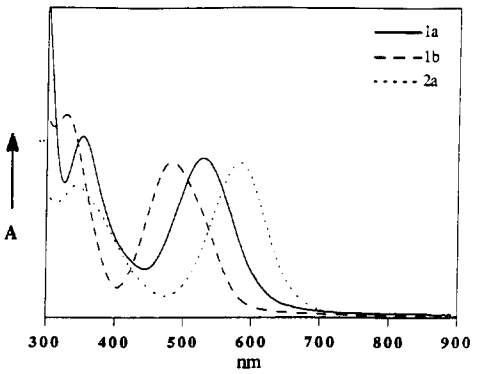

Fig. 2. Electronic absorption spectra of complexes **1a** (———), **1b** (— — —) and **2a** (· · · · · ·) in THF.

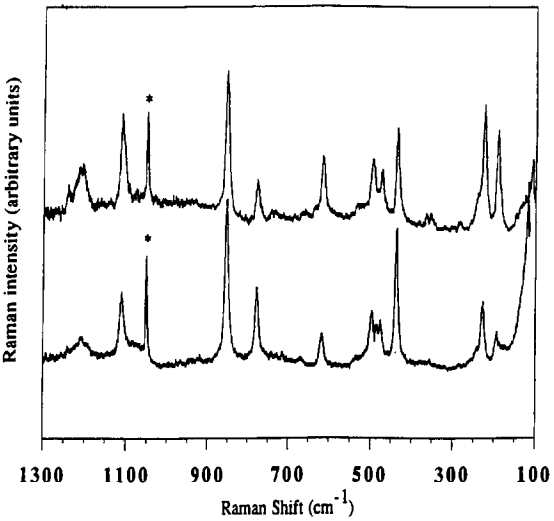

Fig. 3. Part of the resonance Raman spectra of **1b** obtained by excitation of the complex in a KNO_3 disc with 458 nm (bottom) and 536 nm (top). * = NO_3^-.

complexes $(CO)_8Mn_2$(R-DAB-*N,N'*) the ligand has, however, two reactive imine groups which can both form a η^2-bond and therefore produce $(CO)_6Mn_2(\mu$-R-DAB-*N,N':N,C,C',N'*) [44]. A similar reaction apparently occurs for complex **2a** although in this case we were able to detect the intermediate product $(CO)_7Mn_2(\mu$-DBSD-*N,N':N,S*).

In conclusion it can be said that complex **2a** is converted into **3** both thermally and photochemically, although these reactions probably proceed by different mechanisms.

TABLE 5. Spectroscopic data for complexes **1**, **2** and **3** and related compounds

Complex		IR ν(CO) (cm^{-1}) [a]	^{1}H-NMR (ppm) [d]	λ_{max} (nm) [a] (Δ^{max}) [j]
DBSD			1.32	
$Mn(CO)_3Br$(DBSD-*N,N'*)	**1a**	2028s 1944s 1929s	1.62	568(60)
$Re(CO)_3Br$(DBSD-*N,N'*)	**1b**	2026s 1930s 1912s	1.58	518(60)
$Mn(CO)_3Br$(^{t}Bu-DAB-*N,N'*) [g]		2021s 1936s 1927s [b]		489 [f]
$Re(CO)_3Br$(^{t}Bu-DAB-*N,N'*) [g]		2025s 1925s 1910s [b]		453 [f]
$(CO)_8Mn_2$(DBSD-*N,N'*)	**2a**	2072s 2015m 1988vs 1964vw 1927w 1913w	1.51	
$(CO)_8MnRe$(DBSD-*N,N'*)	**2b**	2069s 2009m 1997vs 1981vs 1975w 1952vw 1920s	1.42	552
$(CO)_8ReMn$(DBSD-*N,N'*)	**2c**	2070s 2010m 1999vs 1969s 1957w 1937m	1.48	561(65)
$(CO)_8Re_2$(DBSD-*N,N'*)	**2d**	2091s 2024w 1999vs 1973m 1920s 1912m	1.39	
$(CO)_8Mn_2$(^{i}Pr-DAB-*N,N'*) [h]		2067s 2004m 1987vs 1977vs 1920m 1910m		555
$(CO)_7Mn_2(\mu$-DBSD-*N,N':N,S*)		2036m 2003vs 1942s 1935m 1918m		410
$(CO)_7Mn_2(\mu$-^{i}Pr-PyCa-*N,N':N,C*) [i]		2049m 2011s 1995s 1954s 1941m 1924w 1909w	7.89d 6.42m 5.75m 2.96s 2.65sept 1.47d 1.16d [e]	
$(CO)_6Mn_2(\mu$-DBSD-*N,N':N,S,N'*)**3**		2036m 2003s 1941vs 1935s 1918m		410
$(CO)_6Mn_2(\mu$-^{i}Pr-DAB-*N,N':N,C,C',N*) [i]		2030m 1997s 1949s 1933m 1920w 1914w [c]	5.08s 2.40sept 0.99d 0.74d [e]	

[a] In n-hexane, [b] in CH_2Cl_2, [c] in toluene, [d] in $CDCl_3$, [e] in C_6D_6, [f] in C_6H_6, [g] from [24], [h] from [39], [i] from [44], [j] $\Delta^{max} \equiv \sigma^{max}_{CH_3CN} - \sigma^{max}_{n\text{-}C_6H_{14}}$. IR: vs very strong, s strong, m medium, w weak and vw very weak. ^{1}H-NMR: s singlet, d doublet, sept septet, m multiplet.

TABLE 6. The N–S bond lengths and N–S–N bond angles in free and coordinated sulfurdiimine ligands

		NS bond (Å)	NSN angle
Dimethylsulfurdiimine [42]		1.53	113.6
Di-p,p'-tolylsulfurdiimine [41]		1.53 and 1.56	117.2
$PtCl_2(C_2H_4)$(DBSD-*N*) [43]		1.53 and 1.57	113.0
$W(CO)_4$(DBSD-*N,N'*) [40]		1.58 and 1.59	93.4
$(CO)_8Mn_2$(DBSD-*N,N'*)	**2a**	1.60 and 1.60	94.0
$(CO)_6Mn_2$(μ-DBSD-*N,N':N,S,N'*)	**3**	1.68 and 1.70	85.2

3.4. Crystal structure of 3

ORTEP and PLUTO [37] drawings of the structure of **3** are shown in Fig. 5 and the crystallographic data are listed in Tables 1, 2 and 4. The octahedral geometry of the Mn atoms is much more distorted than in complex **2a**.

The Mn–Mn distance (2.638 Å) is much shorter than that in $Mn_2(CO)_{10}$ (2.9038 Å) [38] and **2a** (2.965 Å) (*vide supra*) and even shorter than that in $(CO)_7Mn_2(\mu$-^{i}Pr-PyCa-*N,N':N,C*) (2.758 Å) [44]. It closely resembles the Mn–Mn distance in the complexes $(CO)_6Mn_2(\mu$-R-DAB-*N,N':N,C,C',N'*) (2.613–2.633 Å) [45,46], in which the R-DAB ligand is σ,σ-coordinated to one Mn atom and η^4 to the other just like the DBSD ligand in the complex under study. Apparently, the Mn–Mn bond length mainly depends on the bonding mode of the sulfurdiimine and α-diimine ligands; it is longest for the unbridged species and becomes shorter and shorter when first one and then two bridging imine or NS groups are introduced. The Mn(2)–CO distances for the three carbonyls that have remained in **3** from the $Mn(CO)_5$ moiety of **2a**, are very similar (1.79–1.81 Å), and nearly equal to the shortest Mn–CO bond distance of that $Mn(CO)_5$ group. The distance between Mn(1) and the axial C(3)O(3) ligand of the Mn(1)$(CO)_3$ group (1.766 Å) is now the shortest Mn–CO bond length in **3**. The N–S bond distances have increased from ~1.60 to ~1.70 Å relative to those in **2a** and this is, of course, to be

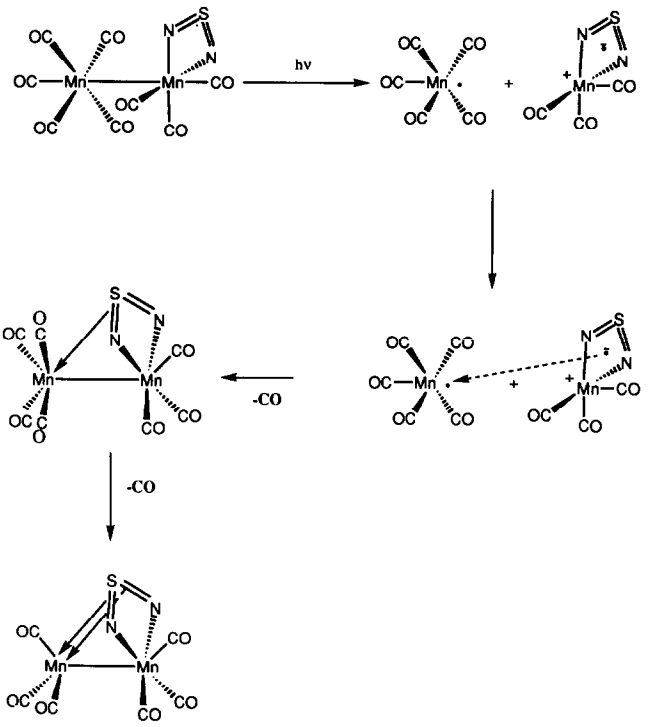

Scheme 1.

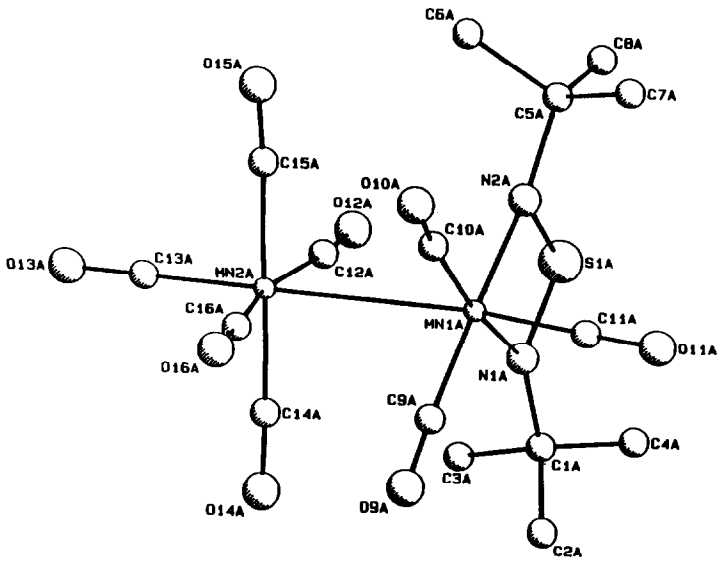

Fig. 4. PLUTO (left) and ORTEP (right) drawings of **2a**.

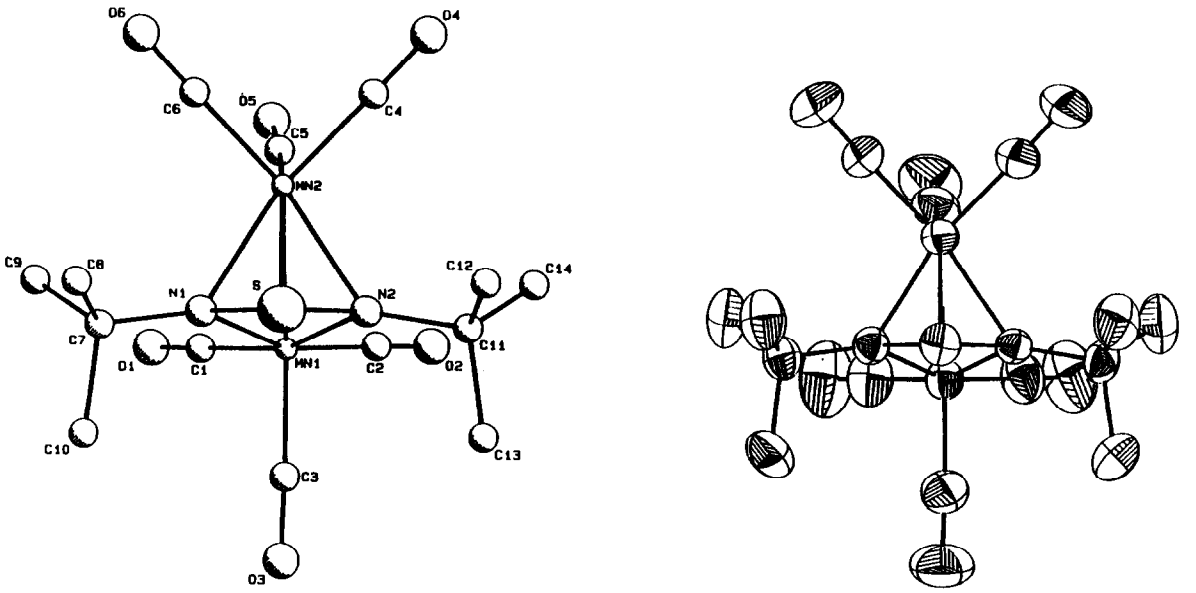

Fig. 5. PLUTO (left) and ORTEP (right) drawings of **3**.

expected when the sulfurdiimine ligand changes its coordination from a four-electron chelate to an eight-electron bridging ligand. It is in fact the longest N–S bond distance observed so far for an intact sulfurdiimine ligand and equals to the N–S bond length in the ^{t}Bu-NS group acting as a bridging six-electron donor ligand in the metal cluster $Fe_3(CO)_9(^t$Bu-NS)(S) [17]. The NSN angle of DBSD (85.2°) is even smaller in this ligand in complex **2a** (94.0°) and about 30° smaller than that in the free ligand (Table 6). The bridging character of the DBSD ligand in this complex is evident from the short Mn(2)–S bond distance (2.218 Å) and from the fact that the Mn(1)–N bond lengths (1.99 Å) are not much longer than the Mn(2)–N bond lengths (2.08 Å).

4. Conclusion

The results show that, starting from the metal–metal bonded complexes $(CO)_8MM'$(DBSD-*N,N'*) (M,M' = Mn, Re), novel complexes of the type $(CO)_6MM'(\mu$-DBSD-*N,N':N,S,N'*) can be prepared in which the sulfurdiimine coordinates as an eight-electron donor ligand to M and M'. The ligand coordinated in this way shows the longest N–S bond distances observed so far for an intact sulfurdiimine.

Acknowledgments

The Netherlands Foundation for Chemical Research (SON) and the Netherlands Organisation for the Advancement of Pure Research (NWO) are thanked for their financial support. We thank Th. Snoeck for recording the Raman spectra, C. Kleverlaan and A. Terpstra for their assistance and help in connection with the UV spectral data.

References

1 K. Vrieze and G. van Koten, Sulfurdiimine, Triazenido, Azabutadiene and Triatomic Hetero Anion Ligands, in G. Wilkinson (ed.), *Comprehensive Coordination Chemistry*, Pergamon Press, Oxford, 1987, p. 189.
2 G. van Koten and K. Vrieze, *Recl. Trav. Chim. Pays-Bas, 100* (1981) 129.
3 G. van Koten and K. Vrieze, *Adv. Organomet. Chem., 21* (1982) 151.
4 K. Vrieze and G. van Koten, *Inorg. Chim. Acta, 100* (1985) 79.
5 K. Vrieze, *J. Organomet. Chem., 300* (1986) 307.
6 D.J. Stufkens, *Coord. Chem. Rev., 104* (1990) 39.
7 K. Vrieze and G. van Koten, *Recl. Trav. Chim. Pays-Bas, 99* (1980) 145.
8 J. Keijsper, H. van der Poel, L.H. Polm, G. van Koten and K. Vrieze, *Polyhedron, 2* (1983) 1111.
9 J. Keijsper, L.H. Polm, G. van Koten, K. Vrieze, G. Abbel and C.H. Stam, *Organometallics, 4* (1983) 2142.
10 J. Keijsper, L.H. Polm, G. van Koten, K. Vrieze, F.A.B. Seignette and C.H. Stam, *Inorg. Chem., 24* (1985) 518.
11 H. van der Poel, G. van Koten, K. Vrieze, M.W. Kokkes and C.H. Stam, *Inorg. Chim. Acta, 39* (1980) 197.
12 H. van der Poel, G. van Koten, M.W. Kokkes and C.H. Stam, *Inorg. Chem., 20* (1981) 2491.
13 H.-W. Frühauf, A. Landers, R. Goddard and C. Krüger, *Angew. Chem., 90* (1978) 56.
14 R. Meij, J. Kuyper, D.J. Stufkens and K. Vrieze, *J. Organomet. Chem., 110* (1976) 219.
15 R. Meij, T.A.M. Kaandorp, D.J. Stufkens and K. Vrieze, *J. Organomet. Chem., 128* (1977) 203.

16 R. Meij, D.J. Stufkens and K. Vrieze, *J. Organomet. Chem., 144* (1978) 239.
17 R. Meij, D.J. Stufkens, K. Vrieze, A.M.F. Brouwers, J.D. Schagen, J.J. Zwinselman, A.R. Overbeek and C.H. Stam, *J. Organomet. Chem., 170* (1979) 337.
18 J. Kuyper and K. Vrieze, *J. Organomet. Chem., 74* (1974) 289.
19 N. Walker and D. Stuart, *Acta Crystallogr., A39* (1983) 158.
20 W.H. Zachariasen, *Acta Crystallogr., A23* (1967) 558.
21 A.C. Larson, The Inclusion of Secondary Extinction in Least-Squares Refinement of Crystal Structures, in F.R. Ahmed, S.R. Hall and C.P. Huber (eds.), *Crystallographic Computing*, Munksgaard, Copenhagen, 1969, p. 291.
22 D.T. Cromer and J.B. Mann, *Acta Crystallogr., A24* (1968) 321; *International Tables for X-ray Crystallography, Vol. IV*, 1974, p. 55, Kynoch Press, Birmingham, U.K.
23 S.R. Hall and J.M. Stewart (eds.), XTAL 3.0 User's Manual (1990), Universities of Western Australia and Maryland.
24 L.H. Staal, A. Oskam and K. Vrieze, *J. Organomet. Chem., 170* (1979) 235.
25 A.J. Graham, B. Akrigg and B. Sheldrick, *Cryst. Struct. Commun., 6* (1977) 571.
26 A.J. Graham, B. Akrigg and B. Sheldrick, *Cryst. Struct. Commun., 6* (1977) 577.
27 G. Schmidt, H. Paulus, R. van Eldik and H. Elias, *Inorg. Chem., 27* (1988) 3211.
28 R.J. Angelici, F. Basolo and A.J. Poë, *J. Am. Chem. Soc., 85* (1963) 2215.
29 L.F. Wuyts and G.P. van der Kelen, *Inorg. Chim. Acta, 23* (1977) 19.
30 A.M. Bond, R. Colton and M.J. McCormick, *Inorg. Chem., 16* (1977) 155.
31 A.M. Bond, R. Colton and M.E. McDonald, *Inorg. Chem., 17* (1978) 2842.
32 G.J. Stor, D.J. Stufkens and A. Oskam, unpublished results.
33 G.J. Stor, D.J. Stufkens and A. Oskam, *Inorg. Chem., 31* (1992) 1318.
34 H.A. Nieuwenhuis, D.J. Stufkens and A. Oskam, unpublished results.
35 C. Mahabiersing and D.J. Stufkens, unpublished results.
36 R.W. Balk, D.J. Stufkens and A. Oskam, *J. Chem. Soc., Dalton Trans.*, (1982) 275.
37 W.D.S. Motherwell and W. Clegg, PLUTO, *Program for plotting molecular and crystal structures*, 1978, University of Cambridge, U.K.
38 M.R. Churchill, K.N. Amoh and H.J. Wasserman, *Inorg. Chem., 20* (1981) 1609.
39 M.W. Kokkes, Th.L. Snoeck, D.J. Stufkens, A. Oskam, M. Christophersen and C.H. Stam, *J. Mol. Struct., 131* (1985) 11.
40 R. Meij and K. Olie, *Cryst. Struct. Commun., 4* (1975) 515.
41 C. Leandri, V. Busetti, G. Valle and M. Mammi, *J. Chem. Soc., Chem. Commun.*, (1970) 413.
42 J. Kuyper, P.H. Isselman and F.C. Mijlhoff, *J. Mol. Struct., 29* (1975) 247.
43 R.T. Kops, E. van Aken and H. Schenk, *Acta Cryst., B29* (1973) 913.
44 T. van der Graaf, D.J. Stufkens, A. Oskam and K. Goubitz, *Inorg. Chem., 30* (1991) 599.
45 R.D. Adams, *J. Am. Chem. Soc., 102* (1980) 7476.
46 P.L. Motz, J.P. Williams, J.J. Alexander, D.M. Ho, J.S. Ricci and W.T. Miller, Jr., *Organometallics, 8* (1989) 1523.